

PP-GWAS: Privacy Preserving Multi-Site Genome-wide Association Studies

Arjhun Swaminathan^{1,2*}, Anika Hannemann^{4,5},
Ali Burak Ünal^{1,2}, Nico Pfeifer^{2,3}, Mete Akgün^{1,2*}

¹Medical Data Privacy and Privacy-preserving Machine Learning
(MDPPML), University of Tübingen, Germany.

²Institute for Bioinformatics and Medical Informatics (IBMI),
University of Tübingen, Germany.

³Methods in Medical Informatics, University of Tübingen, Germany.

⁴Dept. of Computer Science, Leipzig University, Germany.

⁵Center for Scalable Data Analytics and Artificial Intelligence
(ScaDS.AI) Dresden/Leipzig, Germany.

*Corresponding author(s). E-mail(s):

arjhun.swaminathan@uni-tuebingen.de; mete.akguen@uni-tuebingen.de;

Abstract

Genome-wide association studies are pivotal in understanding the genetic underpinnings of complex traits and diseases. Collaborative, multi-site GWAS aim to enhance statistical power but face obstacles due to the sensitive nature of genomic data sharing. Current state-of-the-art methods provide a privacy-focused approach utilizing computationally expensive methods such as Secure Multi-Party Computation and Homomorphic Encryption. In this context, we present a novel algorithm PP-GWAS designed to improve upon existing standards in terms of computational efficiency and scalability without sacrificing data privacy. This algorithm employs randomized encoding within a distributed architecture to perform stacked ridge regression on a Linear Mixed Model to ensure rigorous analysis. Experimental evaluation with real world and synthetic data indicates that PP-GWAS can achieve computational speeds twice as fast as similar state-of-the-art algorithms while using lesser computational resources, all while adhering to a robust security model that caters to an all-but-one semi-honest adversary setting. We have assessed its performance using various datasets, emphasizing its potential in facilitating more efficient and private genomic analyses.

1 Introduction

Genome-wide association studies (GWAS) have emerged as a crucial instrument for discerning the genetic components underpinning complex biological traits and diseases. By investigating differences in allele frequencies of genetic variants, particularly single-nucleotide polymorphisms (SNPs), between ancestrally similar individuals exhibiting distinct phenotypic traits, GWAS have highlighted numerous genomic risk loci associated with a variety of diseases and characteristics [1–3]. The power of these studies is realized especially when multiple datasets are collaboratively analyzed, as such joint efforts have consistently revealed a broader spectrum of associations than when individual datasets are studied in isolation [4, 5].

Nevertheless, despite the potential advantages, multi-site dataset collaborations in the realm of GWAS are rarely realized. This can be attributed predominantly to stringent institutional policies and regulations, such as the GDPR¹ in the European Union, which act as obstacles to the sharing of sensitive genetic data [6]. The emphasis on privacy is not exclusive to the European Union. Other jurisdictions, including in Africa, have started to bolster privacy protections as a response to the growing awareness of the potential misuse of sensitive data [7]. This global move towards stringent data protection presents an important discussion: on one hand, there is the undeniable potential of collaborative GWAS in advancing medical science, and on the other, there is the indispensable need to safeguard individual privacy [8].

The growing interest [9, 10] in secure computation for collaborative multi-site GWAS has led to some state-of-the-art solutions, such as [9], S-GWAS [11] and SF-GWAS [12] that use traditional security techniques. These techniques—Secure-Multi-Party Computation (SMPC) [13], Differential Privacy (DP) [14], and Multiparty-Homomorphic Encryption (MPHE) [15], while secure, introduce practical challenges. For example, SMPC requires frequent and continuous communication, and requires reconfiguration when additional data providers are added to subsequent analyses. Meanwhile DP introduces noise to the analysis that can often be detrimental to model accuracy. Lastly, MPHE demands hospitals and data providers to have access to extensive on-premise computational resources, which is not often the case. Healthcare institutions often rather rely on cloud services for computational tasks [16, 17].

1.1 Our Contributions

With the challenges presented, our work seeks to integrate multi-site GWAS into a distributed architecture where a single third party entity, is tasked with helping the data providers carry out multi-site GWAS in a private and secure manner. We introduce PP-GWAS as an alternative to state-of-the-art solutions, that aims to perform similar computational tasks with high accuracy and reduced computational strain. We evaluate our method against S-GWAS [11] and its more powerful successor, SF-GWAS [12]. Unlike S-GWAS and SF-GWAS that utilize SMPC and MPHE to perform secure multi-site GWAS, our method relies on randomized encoding in a distributed architecture, resulting in improved efficiency and lower computational demands.

¹General Data Protection Regulation

Randomized encoding achieves privacy-preservation by obfuscating data in a lower/higher dimensional space. The encoding is dependent upon the analysis performed on the data, and hence establishing security depends on the encoding used [18]. This often morphs into a dynamic challenge of identifying potential vulnerabilities and attacks rather than proving robustness from the outset. In our work, we use randomized encoding [19, 20] to obfuscate the data, as in other applications such as [21–23].

We adapt a well-established centralized GWAS algorithm based on Linear Mixed Models, REGENIE [24] into a distributed and secure format. We do this since REGENIE is particularly adept at managing large-scale datasets. Importantly, it employs a two-level methodology, where one first performs ridge regression on the whole genome data to arrive at a smaller space of predictions. Subsequently, another round of ridge regression is performed on these predictions in a stacked fashion, and the associated SNPs are individually tested.

We evaluate PP-GWAS against its alternatives on both synthetic data, generated using [25], and two real world datasets: a bladder cancer dataset ($n=13,060$)², and an age-related macular degeneration (AMD) dataset ($n=22,683$)³. Our empirical findings highlight a notable advancement in both scalability and execution speed, with PP-GWAS performing nearly twice as fast as SF-GWAS. Most importantly, these speeds are achieved utilizing computational resources that are considerably lesser than what SF-GWAS necessitates, making our approach more pertinent to real-world scenarios. Moreover, the accuracy of our GWAS results are validated against REGENIE, ensuring comprehensive evaluation.

Further, in terms of the adversarial conditions, SF-GWAS operates within an all-but-one semi-honest adversary framework, and incorporates an external party designated as helper. However, the potential for malicious intent from this external party remains ambiguous. In contrast, our approach distinctly outlines the role of the external party, categorizing it as both non-colluding and semi-honest. This clear description not only ensures the method’s robustness, but also aligns seamlessly with standard privacy enhancing techniques in distributed frameworks [8, 26].

2 Results

2.1 Experimental Setup

Our experiments were conducted on a state-of-the-art high-performance computing (HPC) cluster. Each node within this HPC environment was equipped with an Intel XEON CPU E5-2650 v4, complemented by 256 GB of memory and a 2 TB SSD storage capacity. We employed Python as the primary programming language, taking advantage of Intel’s Math Kernel Library (MKL) for high-demand computational tasks. A dynamic core allocation strategy was utilized for MKL-based operations, enhancing computational efficiency and throughput. To ensure the robustness and reproducibility of our experimental findings, each experiment was conducted five times, and the

²NIH dbGaP accession number phs000346.v2.p2

³NIH dbGaP accession number phs001039.v1.p1

results were averaged. Error bars in the runtime figures represent deviations from these multiple iterations, reflecting the consistency of our measurements.

The architecture of our experimental system was distributed across multiple nodes of the HPC cluster. Individual nodes were allocated for each participant and the server. The server was allowed to access 128GB of memory for all experiments while individual participants utilized memory variably, utilizing up to a maximum of 32GB unless specified otherwise. Such a configuration is reminiscent of real-world scenarios where computational tasks are commonly outsourced by medical and research institutions. This design also mirrors the setup described in SF-GWAS, though with more constrained memory allocations for the participants.

Communication between participants was facilitated through socket programming, implemented using TCP connections. Each participant established a connection to the server through a unique port. The server, leveraging multiprocessing capabilities, managed simultaneous data exchanges with multiple participants. This approach ensured real-time interactions and minimized node idleness. The communication was characterized by a round-trip latency of 0.249ms, with the TCP window size set at the default 128 KByte. For matrix operations, especially involving large sparse datasets, we integrated the sparse-dot-mkl library [27], renowned for its computational efficiency.

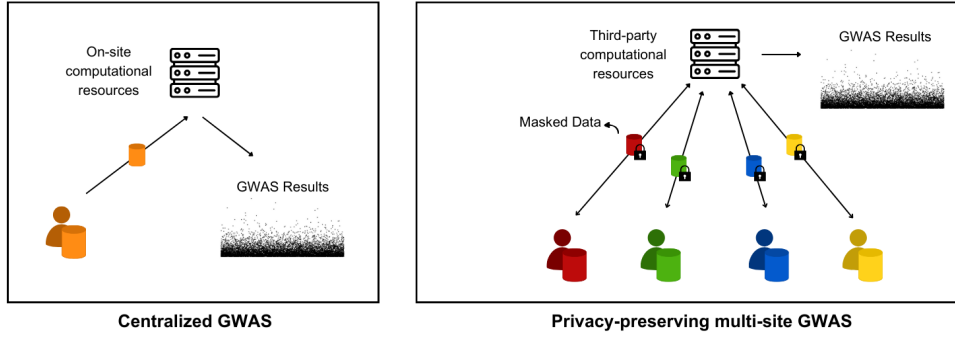


Fig. 1 Comparison of centralised and our privacy-preserving GWAS architectures. On the left, a centralized approach is depicted where a single institution, such as a hospital or research institute, utilizes on-site computational resources to conduct GWAS on its local data. On the right, a distributed model is illustrated, in which multiple entities collaborate to perform GWAS on a combined dataset. This is achieved without sharing the local data, and by leveraging a third-party service to facilitate computations.

In summary, our experimental design was adeptly crafted to leverage the capabilities of the HPC cluster, drawing parallels with the setup detailed in SF-GWAS. By optimizing computational resources and ensuring efficient communication protocols, our aim was to create a robust and versatile system, adept at addressing the stringent demands of genome-wide association studies.

2.2 Data Generation, Storage, and Preprocessing

2.2.1 Synthetic Data Generation

Synthetic data for our experiments was generated using the pysnpools library [25]. The population structure was set at 0.1, and the degree of family relatedness was fixed at 0.25. This synthetic data was horizontally partitioned roughly equally across the participants.

2.2.2 Real Datasets

Two real genomic datasets were used for the experiments: A Bladder Cancer Risk dataset (dbGaP Study Accession: phs000346.v2.p2), and an Age-Related Macular Degeneration dataset (dbGaP Study Accession: phs001039.v1.p1). Access to these datasets was secured through the dbGaP platform, adhering to the necessary procedural requirements. These datasets were further imputed for missing data using Beagle [28].

Both the synthetic and real datasets were further stored blockwise in the .npz format which our program is designed to read.

2.2.3 Quality Control

For both the synthetic and real datasets, a series of preprocessing steps were executed to ensure data quality and relevance. These are a part of the algorithm, and are included in the runtime analysis in the subsequent section. Genotypes with a missing rate exceeding 0.1 were filtered out. Further, only alleles with a minor allele frequency greater than 0.05 were retained. Lastly, a Hardy-Weinberg equilibrium chi-squared test statistic threshold of 23.928 (corresponding to a p-value of 10^{-6}) was applied. It’s noteworthy that these preprocessing measures were securely executed on the whole data by the participants using standard addition-based randomized encoding techniques.

2.3 Accuracy Analysis

To rigorously evaluate the accuracy of PP-GWAS, it was essential to conduct a comparative analysis against the well-established unencrypted plaintext GWAS algorithm, REGENIE. Using Pearson’s r-square coefficient as a measure for accuracy between the negative log of the p-values, PP-GWAS demonstrated robust performance on real-world datasets. Specifically, it achieved an r-square value of 1.00 for both the Bladder Cancer Risk dataset, and the Age-Related Macular Degeneration (AMD) dataset. These outcomes, illustrating high correlation with the plaintext benchmarks, are detailed in Figure 2. This comparison underscores the capability of PP-GWAS to maintain genetic association analysis accuracy while ensuring data privacy.

2.4 Scalability Analysis of PP-GWAS with Simulated Data

The ability to maintain computational efficiency with the large-scale data is a critical challenge in genome-wide association studies. This section provides a comparative analysis between PP-GWAS and the existing state-of-the-art SF-GWAS, focusing on performance under various computational and data conditions.

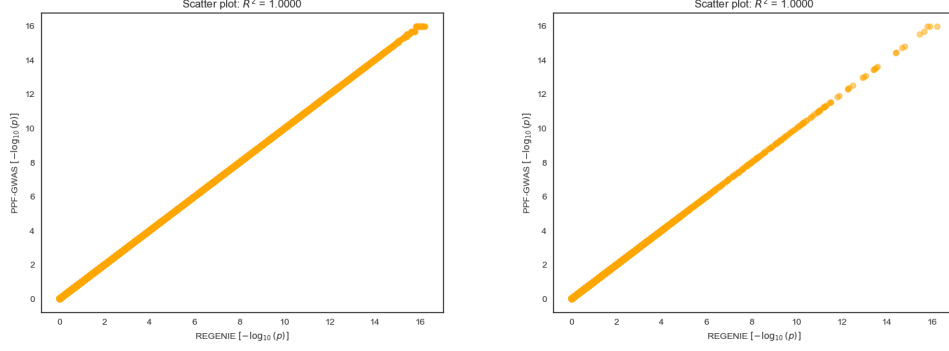


Fig. 2 (a) R-square plot for the Bladder Cancer Risk dataset, illustrating the correlation between the negative logarithm of p-values from PP-GWAS and REGENIE. (b) R-square plot for the Age-Related Macular Degeneration (AMD) dataset, depicting the analogous correlation.

To facilitate a direct comparison, we utilized a simulated dataset designed similar to those in SF-GWAS’s scalability analysis. Such alignment of experimental conditions is crucial to ensure the validity of our performance assessment.

We consider three primary factors in our scalability analysis: the number of computational nodes (referred to as participants), the SNP count within the genomic data, and the sample sizes managed by each node. Incremental increases in each of these factors allow us to observe and quantify the performance implications on PP-GWAS.

Our initial evaluation focuses on the algorithm’s performance in response to an increasing number of participants. With a test dataset comprising 9,178 samples and 612,794 SNPs, we assess the algorithm’s distributed computation capabilities. Performance outcomes, as shown in Figure 3, indicate that PP-GWAS maintains a linear performance with an increasing number of participants, a desirable trait for multi-site GWAS deployments. This is further detailed in Figure 3.

We then explore the scalability in relation to SNP counts, with a fixed configuration of two participants and 9,178 samples. Addressing the large-scale nature of many genomic datasets, PP-GWAS’s performance remains superior to that of SF-GWAS, as depicted in Figure 4.

Lastly, we examine how sample size affects PP-GWAS’s scalability. Keeping the number of participants at two and SNPs constant at 612,794, we increment the sample size and analyze the impact. The robustness of PP-GWAS against increasing computational loads is demonstrated in Figure 5.

In conclusion, the scalability analysis underscores PP-GWAS’s capability to efficiently manage increased computational demands across various dimensions. This is instrumental for its application in extensive genetic association studies.

2.5 Memory Efficiency and Communication Cost Analysis

In the realm of genomic-wide association studies (GWAS), PP-GWAS algorithm presents a notable shift from SF-GWAS, especially in terms of memory efficiency and communication costs. This section goes into how these two critical factors play out in the implementation and scalability of PP-GWAS.

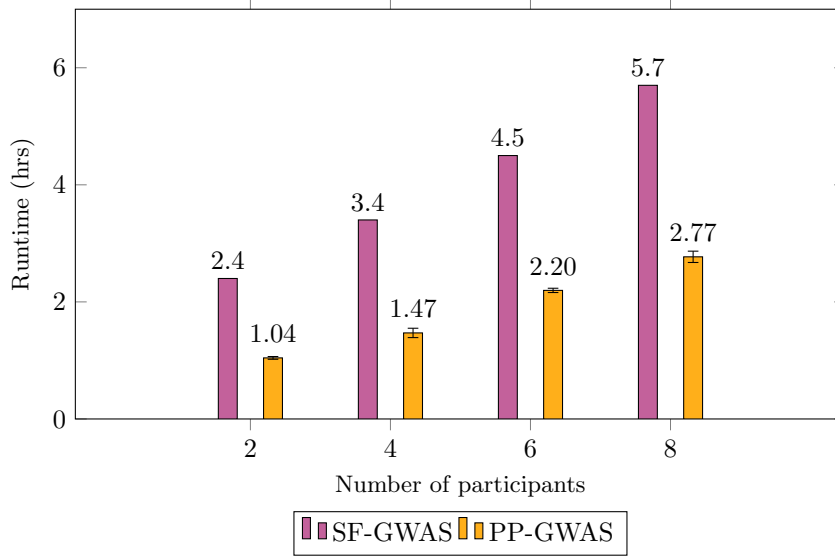


Fig. 3 Comparison of total computational times for SF-GWAS and PP-GWAS, analysing a dataset (9,178 samples \times 612,794 SNPs) across varying number of participating institutions.

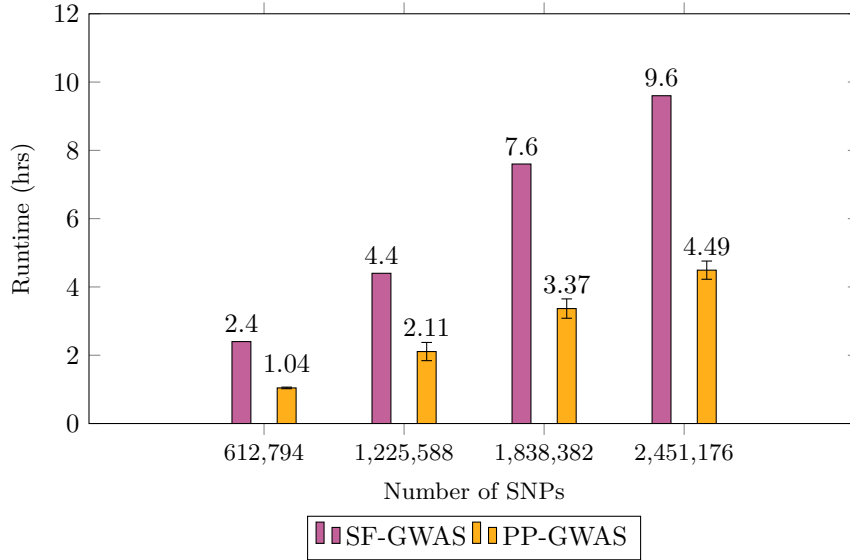


Fig. 4 Comparison of total computational times for SF-GWAS and PP-GWAS, analyzing a dataset with 9,178 samples across two participating institutions, and an increasing number of SNPs.

Memory Efficiency: A key strength of PP-GWAS lies in its significantly reduced RAM requirements compared to SF-GWAS, as discussed in Figure 6. This aspect is particularly advantageous for settings with limited computational resources, such as smaller research institutions or medical facilities. By lowering the memory demands,

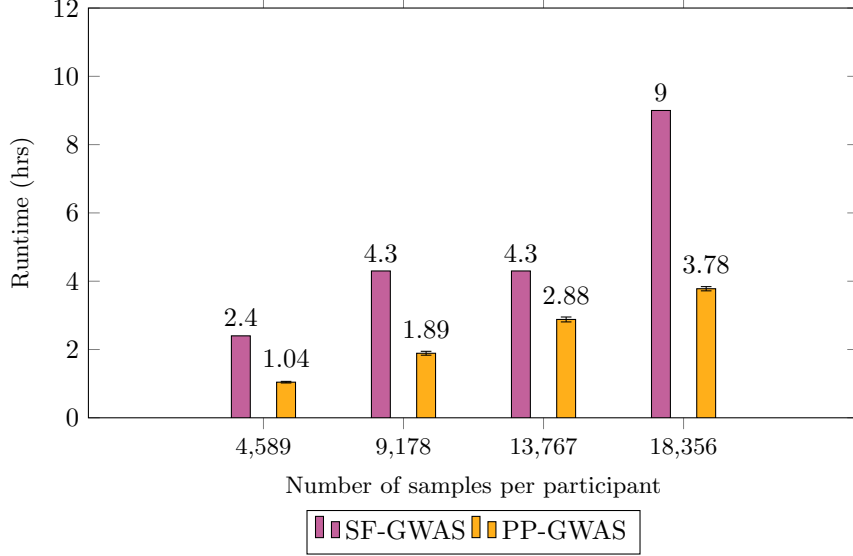


Fig. 5 Comparison of total computational times for SF-GWAS and PP-GWAS, analyzing a dataset with 612,794 SNPs across two participating institutions, and an increasing number of samples.

PP-GWAS enables these organizations to partake in large-scale genetic studies without the need for extensive hardware upgrades. This improvement in memory efficiency is instrumental in democratizing GWAS, allowing for wider and more inclusive research participation.

Communication Costs: While PP-GWAS requires higher communication overhead than SF-GWAS when the number of participants is low, this increase is a strategic trade-off. Specifically, the communication demands in PP-GWAS rise linearly and predictably, in contrast to the exponential growth experienced by SF-GWAS as the number of participants increases. This makes PP-GWAS a more accessible option for many institutions, especially in an era where digital connectivity often surpasses the availability of advanced computational resources. Furthermore, the distributed nature of the PP-GWAS algorithm reduces the number of communication rounds, alleviating some of the burdens seen in SF-GWAS.

2.6 Adaptability to Large-Scale Data

To address the challenge of scaling PP-GWAS to accommodate large-scale genomic datasets, we adopted the use of medium-sized synthetic datasets as representative proxies. This approach was necessitated by the constraints of limited computational resources and the inaccessibility of extensive real-world datasets such as the eMERGE dataset, or the UK Biobank dataset. This approach enabled us to interpolate the amount of time PP-GWAS would need to analyse the datasets. For this purpose, the central server was given access to 256GB of RAM, and the participants, 56GB of RAM. We fixed the number of SNPs arbitrarily to 581927, and scaled up the number of samples, with six participants in the study.

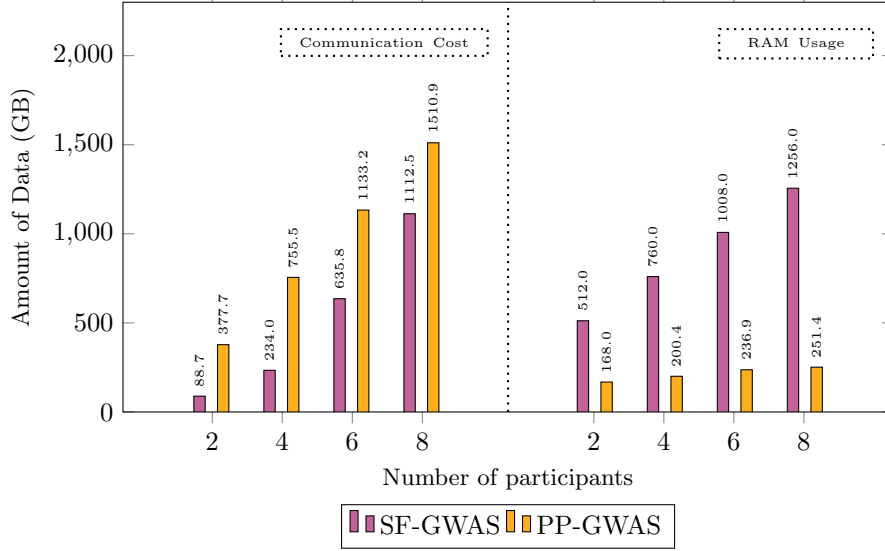


Fig. 6 Comparison of communication cost (in GB), and RAM utility (in GB) across an increasing number of participants, analysing a genetic dataset consisting of 9,178 samples and 612,794 SNPs.

Our results as depicted in Figure 7, use linear extrapolation to predict that PP-GWAS would require approximately 77 hours and 30 minutes to process a dataset comparable in size to the UK Biobank dataset. Further, for the eMERGE dataset, PP-GWAS is projected to complete the task in just 8h 7m.

3 Conclusion

In this study, we introduced PP-GWAS, a privacy-preserving distributed framework designed to perform multi-site genome-wide association studies. Our extensive comparative analysis demonstrates that PP-GWAS maintains genetic association analysis accuracy equivalent to traditional centralised methods, achieving an r-square value of 1.00 against REGENIE, in the analysis of real-world datasets such as the Bladder Cancer Risk dataset, and the Age-Related Macular Degeneration (AMD) dataset.

PP-GWAS excels in scalability and adaptability when tested against the state-of-the-art privacy preserving GWAS algorithm SF-GWAS [12]. Through evaluations with varying number of participants, SNP counts, and sample sizes, our framework demonstrated a consistent linear performance increase, proving its effectiveness in multi-site GWAS deployments. This scalability is essential for accommodating the expanding size and diversity of genomic datasets in real-world scenarios, making PP-GWAS a stable solution even under the constraints of limited computational resources.

Another significant advancement is in memory efficiency and communication costs. PP-GWAS considerably reduces the RAM requirements, enabling institutions with constrained computational resources to participate in genomic research. While it necessitates higher communication overhead than SF-GWAS with less participants, this overhead progresses in a predictable and manageable linear fashion, which is a strategic

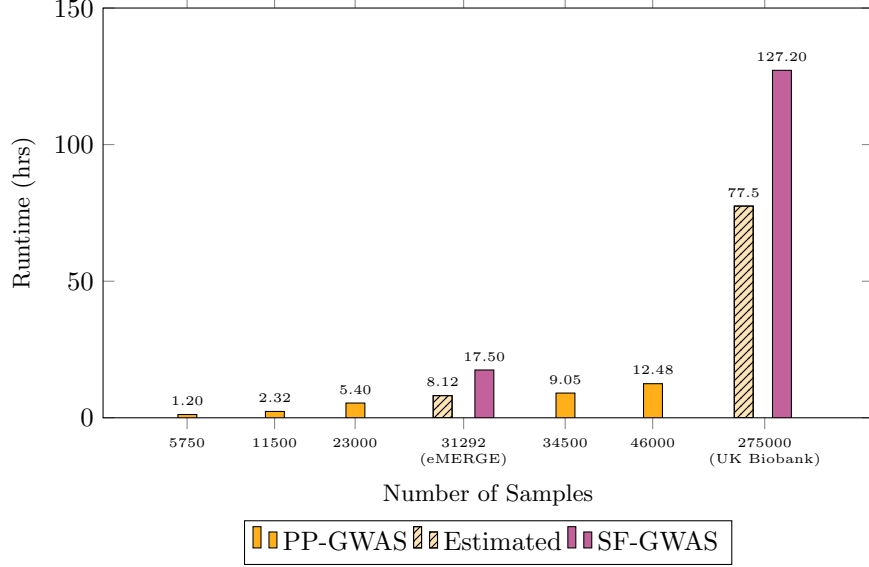


Fig. 7 Comparison of total computational times for PP-GWAS and SF-GWAS when applied to large-scale datasets equivalent in size to the eMERGE and the UK Biobank datasets. PP-GWAS runtimes corresponding to the sizes of these datasets were derived using linear interpolation.

compromise for achieving greater computational and memory efficiency. Further, since the communication overhead for SF-GWAS increases rather exponentially, we expect to perform better with more participants. This trade-off ensures the framework’s applicability across a broader spectrum of research environments, from hospitals to smaller research institutions.

Furthermore, the adaptability of PP-GWAS was tested using medium-sized synthetic datasets as proxies for large-scale datasets, predicting feasible processing times for extensive databases like the eMERGE and the UK Biobank datasets. This adaptability further underscores the potential of PP-GWAS to facilitate large-scale, collaborative, and privacy-sensitive genetic studies, advancing the field of personalized medicine.

In conclusion, PP-GWAS represents a significant step forward in the field of genome-wide association studies. It offers a scalable, accurate, and resource-efficient methodology that respects the privacy of participant data—a balance that is crucial for the future of collaborative medical research.

Supplementary information. Our code is available at the following URL: <https://github.com/mdppml/PPF-GWAS>.

Acknowledgments. This research was supported by the German Ministry of Research and Education (BMBF), project number 01ZZ2010. We express our gratitude to Prof. Dr. rer. nat. Sven Nahnsen for providing access to the real-world datasets utilized in this study. Our gratitude also goes to Dr. Carl Kadie for their assistance in generating synthetic data. Additionally, we acknowledge the usage of the Training Center for Machine Learning (TCML) cluster at the University of Tübingen.

Appendix A Linear Mixed Models in Genome-Wide Association Studies

With regards to GWAS, the application of linear mixed models (LMMs) has emerged as a fundamental approach for deciphering the intricate genetic underpinnings of various phenotypes. A standard linear mixed model used for GWAS is described below.

$$\mathbf{y} = \beta_{\text{test}}\mathbf{x}_{\text{test}} + \mathbf{Z}\boldsymbol{\alpha} + \mathbf{g} + \mathbf{e}, \quad (\text{A1})$$

Here \mathbf{y} represents the phenotype vector of N individuals. The constituents of this model include:

1. **Tested Variant:** \mathbf{x}_{test} encapsulates the minor allele dosages of the variant being tested, represented as 0, 1, or 2, signifying reference-homozygous, heterozygous, and alternate homozygous alleles, respectively. This is represented as a column vector, similar to \mathbf{y} , which are both standardized initially to have mean zero and unit standard deviation.
2. **Covariate:** \mathbf{Z} , an $N \times C$ matrix that accounts for other confounding factors.
3. **Genetic Effects:** The polygenic effect \mathbf{g} includes multiple small-effect size variants, modeled using a Leave-One-Chromosome-Out (LOCO) strategy. Specifically, $\mathbf{g} = \mathbf{X}_{\text{LOCO}}\boldsymbol{\beta}$, with \mathbf{X}_{LOCO} representing the standardized genotypes of m_{LOCO} variants, excluding those from the chromosome of the tested variant.
4. **Environmental Effects:** \mathbf{e} , denoting environmental effects, is modeled as Gaussian noise.

Both \mathbf{x}_{test} and \mathbf{y} are standardized to have zero mean and unit variance. The model incorporates fixed effects (β_{test} and $\boldsymbol{\alpha}$) and random effects (\mathbf{g} and \mathbf{e}). The genetic effect uses what is called the kinship matrix $k = \mathbf{X}_{\text{LOCO}}\mathbf{X}_{\text{LOCO}}^T/m_{\text{LOCO}}$, with $\boldsymbol{\beta} \sim \mathcal{N}(0, (\sigma_g^2/m_{\text{LOCO}})\mathbf{I}_{m_{\text{LOCO}} \times m_{\text{LOCO}}})$, leading to $\mathbf{g} \sim \mathcal{N}(0, \sigma_g^2 k)$. The environmental effect is modeled as $\mathbf{e} \sim \mathcal{N}(0, \sigma_e^2 \mathbf{I}_{n \times n})$. The variance components σ_g^2 and σ_e^2 represent the polygenic and environmental variances, respectively.

The model's validity is assessed by testing the null hypothesis $H_0 : \beta_{\text{test}} = 0$ for each variant, thus identifying significant associations with the phenotype under study.

A pivotal aspect of LMM implementation is the projection of covariates from phenotypes and genotypes, a technique used to remove any confounding effects. This is done by projecting the genomic matrix and the phenotype data to the null space of \mathbf{Z} . The projection matrix is formalized as:

$$\mathbf{P} = \mathbf{I}_n - \mathbf{Z}(\mathbf{Z}^T\mathbf{Z})^{-1}\mathbf{Z}^T,$$

Post-projection, the model assumes the form:

$$\tilde{\mathbf{y}} = \beta_{\text{test}}\tilde{\mathbf{x}}_{\text{test}} + \tilde{\mathbf{X}}_{\text{LOCO}}\boldsymbol{\beta} + \mathbf{e},$$

where $\tilde{\mathbf{y}} = \mathbf{P}\mathbf{y}$, $\tilde{\mathbf{x}}_{\text{test}} = \mathbf{P}\mathbf{x}_{\text{test}}$ and $\tilde{\mathbf{X}}_{\text{LOCO}} = \mathbf{P}\mathbf{X}_{\text{LOCO}}$. This approach effectively removes the influence of covariates, yielding residuals that more accurately reflect the relevant genetic associations.

The LMM-based χ^2 test statistic, central to hypothesis testing, is given by:

$$\chi^2 = \frac{(\tilde{\mathbf{x}}_{\text{test}}^T \mathbf{V}_{\text{LOCO}}^{-1} \tilde{\mathbf{y}})^2}{\tilde{\mathbf{x}}_{\text{test}}^T \mathbf{V}_{\text{LOCO}}^{-1} \tilde{\mathbf{x}}_{\text{test}}},$$

where $\mathbf{V}_{\text{LOCO}} = \hat{\sigma}_g^2 \mathbf{K} + \hat{\sigma}_e^2 \mathbf{I}_{n \times n}$ given the Maximum Likelihood Estimates $\hat{\sigma}_g$ and $\hat{\sigma}_e$ of the variance parameters σ_g and σ_e .

Appendix B Stacked Ridge Regression for LMM-based GWAS

The computation of association statistics within the framework of LMMs presents a significant computational challenge. This complexity arises primarily due to the necessity of maximum likelihood estimation of the variance parameter σ_g , which involves large matrix operations. This complexity escalates dramatically for large-scale datasets, often making the computations prohibitively resource-intensive. Traditional efforts in algorithmic development have primarily focused on optimizing the utilization of the kinship matrix, for instance, through matrix factorization methods.

REGENIE employs a stacked ridge regression strategy and achieves an accuracy comparable to established tools such as BOLT-LMM [29], fastGWA [30], SAIGE [31] and FaST-LMM [32]. Since REGENIE is more friendly to distributed datasets, SF-GWAS employed methods from MPHE and SMPC to build upon the algorithm. We similarly work with REGENIE in a distributed setting.

REGENIE executes its analysis through a methodical two-phased model. The initial phase involves a regression of the contributions from $\tilde{\mathbf{X}}_{\text{LOCO}}$ out of $\tilde{\mathbf{y}}$, followed by fitting β_{test} on these adjusted residuals to ascertain associations. To mitigate the computational demands posed by the extensive genome-wide matrix $\tilde{\mathbf{X}}_{\text{LOCO}}$, REGENIE implements a stacked ridge regression, executed in two distinct phases: Level 0 and Level 1. This approach significantly enhances computational efficiency and adaptability for large-scale genomic datasets, marking a notable progression in the field of genetic association studies.

B.1 Level 0:

At this stage, the genotype matrix \mathbf{X}_{LOCO} is partitioned into B vertical blocks, denoted as

$$\tilde{\mathbf{X}}_{\text{LOCO}} = \left(\tilde{\mathbf{X}}_{\text{LOCO}}^1, \dots, \tilde{\mathbf{X}}_{\text{LOCO}}^B \right).$$

A set of R distinct ridge parameters $\{\lambda_1, \dots, \lambda_R\}$ are then chosen, where

$$\lambda_r := \frac{M(1 - h_r^2)}{h_r^2}, \quad h_r := \frac{0.01(R - 1) + 0.98(r - 1)}{R - 1}.$$

Here, M is the number of SNPs in the study. Consequently, R ridge estimators are computed for each block:

$$\hat{\beta}_{\lambda_r}^b = \left(\left(\tilde{\mathbf{X}}_{\text{LOCO}}^b \right)^T \tilde{\mathbf{X}}_{\text{LOCO}}^b + \lambda_r \mathbf{I}_{n \times n} \right)^{-1} \left(\tilde{\mathbf{X}}_{\text{LOCO}}^b \right)^T \tilde{\mathbf{y}}, \quad (\text{B2})$$

$$\hat{\mathbf{y}}_{\text{LOCO}}^{(b,r)} := \tilde{\mathbf{X}}_{\text{LOCO}}^b \hat{\beta}_{\lambda_r}^b.$$

These intermediate predictors $\hat{\mathbf{y}}_{\text{LOCO}}^{(b,r)}$ for each block are then aggregated into a global feature matrix:

$$\mathbf{W}^b := (\hat{\mathbf{y}}_{\text{LOCO}}^{(b,1)}, \dots, \hat{\mathbf{y}}_{\text{LOCO}}^{(b,R)}), \quad \mathbf{W} := (\mathbf{W}^1, \dots, \mathbf{W}^B). \quad (\text{B3})$$

This is implemented in a k -fold cross validation framework, and hence we denote the k th folds of data as $\tilde{\mathbf{X}}_{(\text{LOCO},k)}^b$ and $\tilde{\mathbf{y}}_{(k)}$, and the data without the k th fold as $\tilde{\mathbf{X}}_{(\text{LOCO},k-1)}^b$ and $\tilde{\mathbf{y}}_{(k-1)}$.

$$\begin{aligned} \hat{\beta}_{(\lambda_r,k-1)}^b &= \left(\left(\tilde{\mathbf{X}}_{(\text{LOCO},k-1)}^b \right)^T \tilde{\mathbf{X}}_{(\text{LOCO},k-1)}^b + \lambda_r \mathbf{I}_{n \times n} \right)^{-1} \left(\tilde{\mathbf{X}}_{(\text{LOCO},k-1)}^b \right)^T \tilde{\mathbf{y}}_{(k-1)}, \\ \hat{\mathbf{y}}_{(\text{LOCO},k)}^{(b,r)} &:= \tilde{\mathbf{X}}_{(\text{LOCO},k)}^b \hat{\beta}_{(\lambda_r,k-1)}^b. \end{aligned}$$

B.2 Level 1:

In this phase, a subsequent round of ridge regression is conducted on the intermediate feature matrix of size $N \times BR$, using R parameters $\{\omega_1, \dots, \omega_R\} = \{(BR/M)\lambda_1, \dots, (BR/M)\lambda_R\}$. The ridge estimators are thus:

$$\hat{\eta}_r = (\mathbf{W}^T \mathbf{W} + \omega_r \mathbf{I}_{BR \times BR})^{-1} \mathbf{W}^T \tilde{\mathbf{y}}.$$

The optimal ridge parameter r^* is selected by minimizing the residual sum of squares:

$$r^* = \arg \min_r \|\tilde{\mathbf{y}} - \mathbf{W} \hat{\eta}_r\|^2. \quad (\text{B4})$$

Phenotype predictions by the stacked regression model are defined as

$$\hat{\mathbf{y}}_{\text{LOCO}} = \mathbf{W} \hat{\eta}_{r^*}.$$

Notably, these two levels of ridge regression are implemented within a k -fold cross-validation framework. The predictions for the k th fold $\hat{\mathbf{y}}_k$ are aggregated, where

$$\begin{aligned} \hat{\mathbf{y}}_k &:= \mathbf{W}_k \hat{\eta}_{(k-1,r^*)}, \\ \hat{\eta}_{(k-1,r)} &:= (\mathbf{W}_{k-1}^T \mathbf{W}_{k-1} + \omega_r \mathbf{I}_{BR \times BR})^{-1} \mathbf{W}_{k-1}^T \tilde{\mathbf{y}}_{k-1}, \\ r^* &= \arg \min_r \sum_k \|\tilde{\mathbf{y}}_k - \mathbf{W}_k \hat{\eta}_{(k-1,r)}\|^2. \end{aligned}$$

The global predictor $\hat{\mathbf{y}} := \sum_k^k \hat{\mathbf{y}}_k$ facilitates the calculation of the associated χ^2 statistic with one degree of freedom for the variant being tested:

$$\chi^2 = \frac{(\tilde{\mathbf{x}}_{\text{test}}^T (\tilde{\mathbf{y}} - \hat{\mathbf{y}}))^2}{\hat{\sigma}_e^2 (\tilde{\mathbf{x}}_{\text{test}}^T \tilde{\mathbf{x}}_{\text{test}})}, \quad \hat{\sigma}_e^2 := \frac{\|\tilde{\mathbf{y}} - \hat{\mathbf{y}}\|_2^2}{(N - C)}.$$

The SNPs that have a χ^2 value of above a significant threshold are taken to be associated with the phenotype. The exact threshold depends on the study [33], with a conventional threshold being a p-value of 5×10^{-8} .

Appendix C Our Privacy-preserving distributed Approach

In our proposed framework, the genomic information X , covariate information Z , and phenotype information y are horizontally partitioned across P participants, with each party p holding X_p , Z_p , and y_p . Each party maintains a count of the total number of samples added to the study prior to their inclusion and the overall sample count. This information is conveyed through a sequential onboarding process. Upon joining the study, the first party shares their sample count with the next party, and the second party learns the cumulative sample count. At the outset of the study, all participants establish a shared secret key, k_{seed} , unknown to the server. This secret key serves as the seed for generating subsequent shared keys. We denote that we have N samples in total, M SNPs, C covariates, and B blocks, of which, M , C and B can be inferred by the server.

C.1 Quality Control

In our protocol, the initial stage involves rigorous quality control (QC) checks on the genetic data obtained from various sources. This step is crucial to ensure the data's integrity and reliability, which are foundational for the accuracy of subsequent genetic analyses. We adhere to stringent criteria for these checks: a missing rate below 0.1, a minor allele frequency (MAF) above 0.05, and a Hardy-Weinberg equilibrium (HWE) chi-squared test statistic threshold of 23.928. These thresholds are aligned with established GWAS standards, allowing us to filter Single Nucleotide Polymorphisms (SNPs) effectively. Consistent with existing policies, for instance by the National Institutes for Health (NIH)⁴, our process includes sharing the total counts of reference homozygous, heterozygous, and alternate homozygous alleles for each SNP with each participating party, a practice also mirrored in SF-GWAS. Additionally, one could safeguard this sensitive statistical data using differential privacy techniques, which impose a minimal additional overhead.

To preserve data confidentiality during the QC phase in our distributed environment, since we only need to sum the totals amongst all participants, we implement simple addition based randomized encoding in a server-assisted manner. While Multi-Party Computation (MPC) could be used to ascertain allele frequencies, our approach

⁴NIH Genomic Data Sharing Policy

leverages the existing centralized server to reduce communication overhead, optimizing the process within the constraints of our architecture.

C.2 Distributed Projection of Covariates and Standardizing

Subsequently, we standardize the genomic matrix \mathbf{X} and phenotype matrix \mathbf{y} , and project out covariate information \mathbf{Z} in the same computation. We do this by appending \mathbf{Z} with a column of ones to mean-center \mathbf{X} and \mathbf{y} . We shall denote the updated covariate matrix as \mathbf{Z}_1 . We also pre-compute the standard deviation matrix $S_{\mathbf{X}}$ of \mathbf{X} and the standard deviation $s_{\mathbf{y}}$ of phenotype information \mathbf{y} using the same addition-based randomized encoding approach as before, since we only need to sum up relevant allele counts from each party. We can then project out covariates in a single computation since we know that

$$(I_N - \mathbf{Z}(\mathbf{Z}^T \mathbf{Z})^{-1} \mathbf{Z}^T) \mathbf{X}_S = (I_N - \mathbf{Z}_1(\mathbf{Z}_1^T \mathbf{Z}_1)^{-1} \mathbf{Z}_1^T) \mathbf{X} S_{\mathbf{X}}.$$

Here \mathbf{X}_S denotes \mathbf{X} after standardization. To perform this computation in a distributed manner, we adopt methods based on randomized projection from [19], where we achieve data obfuscation using a unitary transformation of \mathbf{Z} denoted by $O_{\mathbf{Z}} \mathbf{Z}$ where $O_{\mathbf{Z}}^\dagger O_{\mathbf{Z}} = I = O_{\mathbf{Z}} O_{\mathbf{Z}}^\dagger$. However, some approximation could be achieved with reconstruction attacks, where one can closely recover \mathbf{Z} with an approximation $\tilde{\mathbf{Z}}$ of \mathbf{Z} by solving the orthogonal procrustes problem given by

$$\operatorname{argmin}_O \|O \tilde{\mathbf{Z}} - (O_{\mathbf{Z}} \mathbf{Z})\|_2, \quad O^\dagger O = I.$$

It is also highlighted in [19] that independent component analysis [34, 35] can be performed on the problem to recover hidden factors that help reconstruct the original input. Hence, to thwart such attempts, we require $O_{\mathbf{Z}}$ to not only satisfy $E[O_{\mathbf{Z}}^\dagger O_{\mathbf{Z}}] = I$, but to also be rectangular since the unbalanced orthogonal procrustes problem is unsolved [36]. Hence to obscure \mathbf{X} and \mathbf{y} in this stage, we follow methods from [19, 23, 37], and apply a triple matrix masking such that we have $O_{\mathbf{Z}} \mathbf{X} O_{\mathbf{X}}^\dagger$ and $k_1 O_{\mathbf{Z}} \mathbf{y}$. Here $O_{\mathbf{X}}$ and $O_{\mathbf{Z}}$ are rectangular and satisfy $E[O_{\mathbf{X}}^\dagger O_{\mathbf{X}}] = I = E[O_{\mathbf{Z}}^\dagger O_{\mathbf{Z}}]$. Here k_1 is a random constant.

Hence, each participant p prepares encoded data in the form of $O_{\mathbf{Z}} \mathbf{Z}_p, O_{\mathbf{Z}} \mathbf{X}_p O_{\mathbf{X}}^\dagger$, and $k_1 O_{\mathbf{Z}} \mathbf{y}_p$. We note that $O_{\mathbf{Z}}, O_{\mathbf{X}}$ and k_1 are generated by all participants using the shared seed k_{seed} . The server then computes for each party,

$$\begin{aligned} O_{\mathbf{Z}} \tilde{\mathbf{X}}_p S_{\tilde{\mathbf{X}}}^{-1} O_{\tilde{\mathbf{X}}}^\dagger &= O_{\mathbf{Z}} \mathbf{X}_p O_{\mathbf{X}}^\dagger - O_{\mathbf{Z}} \mathbf{Z}_p ((O_{\mathbf{Z}} \mathbf{Z})^\dagger (O_{\mathbf{Z}} \mathbf{Z}))^{-1} (O_{\mathbf{Z}} \mathbf{Z})^\dagger \sum_p (O_{\mathbf{Z}} \mathbf{X}_p O_{\mathbf{X}}^\dagger), \\ O_{\mathbf{Z}} \mathbf{Z} &= \sum_p (O_{\mathbf{Z}} \mathbf{Z}_p). \end{aligned}$$

The participants can then compute

$$E[\tilde{\mathbf{X}}_p] = O_{\mathbf{Z}}^\dagger (O_{\mathbf{Z}} \tilde{\mathbf{X}}_p S_{\tilde{\mathbf{X}}}^{-1} O_{\tilde{\mathbf{X}}}^\dagger) O_{\tilde{\mathbf{X}}} S_{\mathbf{X}}.$$

Analogously, the participants compute $E[\tilde{\mathbf{y}}_p]$.

C.3 Level 0 Ridge Regression using distributed ADMM

Next, we would like to perform the first level of ridge regression on the genotypes against the phenotypes, using R parameters $(\lambda_1, \dots, \lambda_R)$ given by

$$\lambda_r := \frac{M(1 - h_r^2)}{h_r^2}, \quad h_r := \frac{0.01(R - 1) + 0.98(r - 1)}{R - 1}.$$

We now estimate $\hat{\beta}_{\lambda_r}^b$ for all blocks b from B2. For this purpose, we adopt the distributed Alternate Direction Method of Multipliers from [38] to jointly estimate the level 0 predictions. Note that on a centralized dataset, the ridge regression problem can be formulated as the following optimization problem for a given ridge parameter λ_r .

$$\hat{\beta}_{\lambda_r}^b = \operatorname{argmin}_{\beta} \left(\|\tilde{\mathbf{X}}^b \beta - \tilde{\mathbf{y}}\|_2^2 + \lambda_r \|\beta\|_2^2 \right). \quad (\text{C5})$$

We introduce a variable \mathbf{b} to rewrite C5 as a constraint problem below.

$$\begin{aligned} \hat{\beta}_{\lambda_r}^b &= \operatorname{argmin}_{\beta, \mathbf{b}} \left(\|\tilde{\mathbf{X}}^b \beta - \tilde{\mathbf{y}}\|_2^2 + \lambda_r \|\mathbf{b}\|_2^2 \right), \\ \beta - \mathbf{b} &= 0. \end{aligned} \quad (\text{C6})$$

Since the data in our setting is horizontally partitioned, we can rewrite C6 as follows, where we also horizontally partition β .

$$\begin{aligned} \hat{\beta}_{\lambda_r}^b &= \operatorname{argmin}_{\beta_p, \mathbf{b}} \left(\sum_{p=1}^P \|\tilde{\mathbf{X}}_p^b \beta_p - \tilde{\mathbf{y}}\|_2^2 + \lambda_r \|\mathbf{b}\|_2^2 \right), \\ \beta_p - \mathbf{b} &= 0 \quad \forall p. \end{aligned} \quad (\text{C7})$$

Hence, we detail our distributed approach to use randomized encoding of the input data to compute C7 in Algorithm 1 below. The participants use their shared seed to consistently segregate their data into B blocks. They also then use the seed to determine how they split their data vertically into K folds, such that every participant has some data in every fold. They then denote the k th fold as $\tilde{\mathbf{X}}_{(p,k)}^b$ and the data without the k th fold as $\tilde{\mathbf{X}}_{(p,k-1)}^b$. Similarly, they have $\tilde{\mathbf{y}}_{(p,k)}$ and $\tilde{\mathbf{y}}_{(p,k-1)}$.

C.4 Level 1 Ridge Regression using distributed CGD

Now, like before in the centralized formulation as in B3, we have reduced our problem to lower dimensionality. We then perform Conjugate Gradient descent, however on the server's side on the obfuscated data, as described in Algorithm 2 below. For this, the server prepares R ridge regression parameters $(\omega_1, \dots, \omega_R)$ given by

$$\omega_r := \frac{BR(1 - h_r^2)}{h_r^2}, \quad h_r = \frac{0.01(R - 1) + 0.98(r - 1)}{R - 1}.$$

Algorithm 1 Distributed ADMM Algorithm for Level 0 Ridge Regression

Input: Each party p in $\{1, \dots, P\}$ knows matrices $\tilde{\mathbf{X}}_{(p,k)}^b$, $\tilde{\mathbf{X}}_{(p,k-1)}^b$, column vector $\tilde{\mathbf{y}}_{(p,k-1)}$, learning rate l , and the number of ridge regression parameters R . The server requires learning rate l , ridge regression parameters $\{\lambda_1, \dots, \lambda_R\}$, and number of iterations n .

Output: Obfuscated Level 0 predictions for block b , regression parameter λ_r , and fold k given by $O_{\tilde{\mathbf{y}}}^{(k,r)} \hat{\mathbf{y}}_k^{(b,r)}$.

1. Each party, using a shared seed, prepares a non-zero constant $k_{\tilde{\mathbf{y}}}$, rectangular matrices $O_{\tilde{\mathbf{y}}}^{(k,r)}$, $O_{\tilde{\mathbf{X}}}^{(k,b,r)}$ for all k, b, r , ensuring $E[(O_{\tilde{\mathbf{y}}}^{(k,r)})^\dagger O_{\tilde{\mathbf{y}}}^{(k,r)}] = I_N$ and $E[(O_{\tilde{\mathbf{X}}}^{(k,b,r)})^\dagger O_{\tilde{\mathbf{X}}}^{(k,b,r)}] = I_{N_b}$.
2. For each combination of k, b, r :
 - (a) Server initializes $^{(0)}, {}^{(0)}, {}^{(0)}$ to 0.
 - (b) Participants compute and share with the server:
 - $\mathcal{R}^{(p,k,b,r)} := O_{\tilde{\mathbf{X}}}^{(k,b,r)} \left[(\tilde{\mathbf{X}}_{(p,k-1)}^b)^T (\tilde{\mathbf{X}}_{(p,k-1)}^b) + l I_{N_b} \right] (O_{\tilde{\mathbf{X}}}^{(k,b,r)})^\dagger$,
 - $\mathcal{X}^{(p,k,b,r)} := \frac{1}{k_{\tilde{\mathbf{y}}}} (O_{\tilde{\mathbf{y}}}^{(k,r)})^\dagger \tilde{\mathbf{X}}_{(p,k)}^b O_{\tilde{\mathbf{X}}}^{(k,b,r)}$,
 - $\mathcal{Y}^{(p,k,r)} := k_{\tilde{\mathbf{y}}}^2 O_{\tilde{\mathbf{y}}}^{(k,r)} \tilde{\mathbf{y}}_{(k)}$,
 - (c) Server computes:
 - ${}_p^{(1)} = \mathcal{R}^{(p,k,b,r)} \left(\sum_{\hat{k} \neq k} \mathcal{X}^{(p,\hat{k},b,r)} \right)^\dagger \mathcal{Y}^{(p,k,r)}$,
 - ${}^{(1)} = \sum_p {}_p^{(1)} / P$,
 - ${}^{(1)} = l^{(1)} / \lambda_r$,
 - ${}_p^{(1)} = l \left({}_p^{(1)} - {}^{(1)} \right)$,
 - ${}^{(1)} = \sum_p {}_p^{(1)}$.
 - (d) For i in $\{1, \dots, n-1\}$:
 - Server updates as follows:
 - ${}_p^{(i+1)} = \mathcal{R}^{(p,k,b,r)} \left(\left(\sum_{\hat{k} \neq k} \mathcal{X}^{(p,\hat{k},b,r)} \right)^\dagger \left(\sum_{\hat{k} \neq k} \mathcal{Y}^{(p,\hat{k},r)} \right) + l^{(i)} - {}_p^{(i)} \right)$,
 - ${}^{(i+1)} = \sum_p {}_p^{(i+1)} / P$,
 - ${}^{(i+1)} = l^{(i+1)} + {}^{(i)} / \lambda_r$,
 - ${}_p^{(i+1)} = {}^{(i)} + l \left({}_p^{(i+1)} - {}^{(i+1)} \right)$,
 - ${}^{(i+1)} = \sum_p {}_p^{(i+1)}$.
 - (e) Server computes $\mathcal{X}^{(p,k,b,r)(n)} = O_{\tilde{\mathbf{y}}}^{(k,r)} \hat{\mathbf{y}}_k^{(b,r)}$.

Return: $O_{\tilde{\mathbf{y}}}^{(k,r)} \hat{\mathbf{y}}_k^{(b,r)}$.

C.5 Distributed Single SNP Association Testing

For the association testing stage of the of the analyses, the participants engage in a one-off communication with the server, helping them retrieve the χ^2 values associated with each SNP. This is outlined in Algorithm 3 below.

Algorithm 2 CGD Algorithm for Level 1 Ridge Regression

Input: The server requires a number of iterations n , ridge regression parameters $\{\omega_1, \dots, \omega_R\}$, pre-received $\mathcal{Y}^{(p,k,r)}$ from the level 0 computation and the precomputed $O_{\hat{\mathbf{y}}}^{(k,r)} \hat{\mathbf{y}}_k^{(b,r)}$ for all k, b, r .

Output: Obfuscated Level 1 predictions for regression parameter ω_r , and fold k given by $k_{\hat{\mathbf{y}}}^2 O_{\hat{\mathbf{y}}}^{(k,r)} [\hat{\mathbf{y}}_k^{(1,r)}, \dots, \hat{\mathbf{y}}_k^{(B,r)}] \hat{\eta}_{(k-1,r)}$.

1. For each combination of k, r :

(a) Server initializes $^{(0)}$ to 0.

(b) Server initializes $^{(0)}, ^{(0)}$ to $\sum_{\hat{k} \neq k} \left(\left(O_{\hat{\mathbf{y}}}^{(\hat{k},r)} \hat{\mathbf{y}}_{\hat{k}}^{(b,r)} \right)^\dagger \left(\sum_p \mathcal{Y}^{(p,\hat{k},r)} \right) \right)$.

(c) Server precomputes $\mathcal{W} = \sum_{\hat{k} \neq k} \left(O_{\hat{\mathbf{y}}}^{(\hat{k},r)} \hat{\mathbf{y}}_{\hat{k}}^{(b,r)} \right)^\dagger \left(O_{\hat{\mathbf{y}}}^{(\hat{k},r)} \hat{\mathbf{y}}_{\hat{k}}^{(b,r)} \right)$.

(d) For i in $\{0, \dots, n-1\}$: Server updates as follows:

- $\alpha = \mathcal{W}^{(i)}$,
- $\beta = \alpha + \omega_r^{(i)}$,
- $\gamma = ((^{(i)})^\dagger)^{(i)} / (^{(i)}) \alpha$,
- $^{(i+1)} = i + \gamma^{(i)}$,
- $^{(i+1)} = ^{(i)} - \gamma \alpha$,
- $\delta = ((^{(i+1)})^\dagger)^{(i+1)} / ((^{(i)})^\dagger)^{(i)}$,
- $^{(i+1)} = ^{(i)} + \delta^{(i)}$.

(e) Server computes:

$$r^* := \sum_k \operatorname{argmin}_r \left\| \sum_p \bar{\mathcal{Y}}^{(p,k,r)} - k_{\hat{\mathbf{y}}}^2 O_{\hat{\mathbf{y}}}^{(k,r)} [\hat{\mathbf{y}}_k^{(1,r)}, \dots, \hat{\mathbf{y}}_k^{(B,r)}] \hat{\eta}_{(k-1,r)} \right\|_2^2.$$

Return: $O_{\hat{\mathbf{y}}}^{(k,r^*)} [\hat{\mathbf{y}}_k^{(1,r^*)}, \dots, \hat{\mathbf{y}}_k^{(B,r^*)}]^{(n)} = k_{\hat{\mathbf{y}}}^2 O_{\hat{\mathbf{y}}}^{(k,r^*)} [\hat{\mathbf{y}}_k^{(1,r^*)}, \dots, \hat{\mathbf{y}}_k^{(B,r^*)}] \hat{\eta}_{(k-1,r^*)}$.

C.6 Privacy Analysis

In the section that follows, we explore the privacy guarantees of our algorithm within an adversarial framework, comprising a subset of semi-honest participants and/or a semi-honest non-colluding central server. We establish that the privacy of genetic data held by the participants is preserved. Specifically, we demonstrate that a corrupted participant is unable to extract any information about the data of other non-corrupted participants, and similarly, a corrupted server is incapable of deducing any participant-specific information. It is important to clarify that our analysis does not cover extreme data scenarios, that automatically enable the prediction of number of samples and block sizes. Our proof methodology aligns with the approaches documented in prior works [19, 23, 37, 39, 40].

Theorem 1. *The proposed methodology is secure against a semi-honest adversary who corrupts the central server.*

Proof. We define a semi-honest central server to be a third-party computational service that adheres to the prescribed protocol, but attempts to learn the private data. In our methodology, the server receives encoded data $O_{\mathbf{Z}} \mathbf{Z}_p \in \mathbb{C}^{(N+k\mathbf{z}) \times C}$, $O_{\mathbf{Z}} \mathbf{X}_p O_{\mathbf{X}}^\dagger \in$

Algorithm 3 Distributed Association Testing

Input: The server requires pre-received $\tilde{\mathbf{y}}^{(p,k,r)}$ from the level 0 computation and the precomputed $\mathcal{K}_k := k_{\tilde{\mathbf{y}}}^2 O_{\tilde{\mathbf{y}}}^{(k,r^*)} [\hat{\mathbf{y}}_k^{(1,r^*)}, \dots, \hat{\mathbf{y}}_k^{(B,r^*)}] \hat{\eta}_{(k-1,r^*)}$ from the level 1 computation for all k .

Output: χ^2 value associated to SNP $\tilde{\mathbf{x}}_{test}$.

1. Participants prepare a common non-zero constant $k_{\mathbf{x}}$ for SNP \mathbf{x}_{test} using the shared seed k_{seed} .
2. Participants compute and share $k_{\mathbf{x}} \left(O_{\tilde{\mathbf{y}}}^{(k,r^*)} \right)^\dagger \tilde{\mathbf{x}}_{(test,k,p)}$ for all k .
3. Server computes

$$\chi_{\mathbf{x}_{test}}^2 = \frac{\left[\sum_k \left(\sum_p k_{\mathbf{x}} \left(O_{\tilde{\mathbf{y}}}^{(k,r^*)} \right)^\dagger \tilde{\mathbf{x}}_{(test,k,p)} \right)^\dagger \left(\sum_p \mathcal{Y}^{(p,k,r)} - \mathcal{K}_k \right) \right]^2}{\hat{\sigma}^2 \sum_p \left(k_{\mathbf{x}} \left(O_{\tilde{\mathbf{y}}}^{(k,r^*)} \right)^\dagger \tilde{\mathbf{x}}_{(test,k,p)} \right)^\dagger \left(k_{\mathbf{x}} \left(O_{\tilde{\mathbf{y}}}^{(k,r^*)} \right)^\dagger \tilde{\mathbf{x}}_{(test,k,p)} \right)},$$

where

$$\hat{\sigma}^2 = \frac{1}{N-C} \sum_k \left\| \sum_p \mathcal{Y}^{p,k,r^*} - \mathcal{K}_k \right\|^2.$$

Return: $\chi_{\mathbf{x}_{test}}^2$.

$\mathbb{C}^{(N+k_{\mathbf{z}}) \times (N+k_{\mathbf{x}})}$, $k_1 O_{\mathbf{Z}} \mathbf{y}_p \in \mathbb{C}^{(N+k_{\mathbf{z}}) \times 1}$, and $k_{\mathbf{x}} \left(O_{\tilde{\mathbf{y}}}^{(k,r^*)} \right)^\dagger \tilde{\mathbf{x}}_{(test,k,p)} \in \mathbb{C}^{(N+k_{\mathbf{x}}) \times 1}$ from each input party where N is the number of samples and C is the number of covariates. The data the central server then has access to includes

1. $O_{\mathbf{Z}} \mathbf{Z}_p, O_{\mathbf{Z}} \mathbf{X}_p O_{\mathbf{X}}^\dagger, k_1 O_{\mathbf{Z}} \mathbf{y}_p$, and $k_{\mathbf{x}} \left(O_{\tilde{\mathbf{y}}}^{(k,r^*)} \right)^\dagger \tilde{\mathbf{x}}_{(test,k,p)}$.
2. $\mathbf{Z}_p^T \mathbf{Z}_p$, and analogously $k_1^2 \mathbf{y}_p^T \mathbf{y}_p$ and $k_{\mathbf{x}}^2 \tilde{\mathbf{x}}_{(test,k,p)}^T \tilde{\mathbf{x}}_{(test,k,p)}$.

Regarding 1, it is evident that the number of samples, and the block sizes are hidden from the central server. Now we show that $O_{\mathbf{Z}} \mathbf{Z}_p$ is not produced by a unique pair $O_{\mathbf{Z}}$ and \mathbf{Z}_p . Given a unitary matrix $U \in \mathbb{C}^{N \times N}$, $\tilde{O}_{\mathbf{Z}} = O_{\mathbf{Z}} U^\dagger$, and $\tilde{\mathbf{Z}}_p = U \mathbf{Z}_p$, we have $O_{\mathbf{Z}} \mathbf{Z}_p = \tilde{O}_{\mathbf{Z}} \tilde{\mathbf{Z}}_p$. Analogous arguments hold for $O_{\mathbf{Z}} \mathbf{X}_p O_{\mathbf{X}}^\dagger, k_1 O_{\mathbf{Z}} \mathbf{y}_p$, and $k_{\mathbf{x}} \left(O_{\tilde{\mathbf{y}}}^{(k,r^*)} \right)^\dagger \tilde{\mathbf{x}}_{(test,k,p)}$.

If the server wants to perform a reconstruction attack using similar data $\hat{\mathbf{Z}}_p$, which is drawn from a distribution similar to \mathbf{Z}_p , they would want to find a transformation matrix L such that $L O_{\mathbf{Z}} \mathbf{Z}_p = \hat{\mathbf{Z}}$. However, since the number of samples N is unknown to the server, and $\hat{\mathbf{Z}}_p$ and \mathbf{Z}_p exist in different spaces, the approximation is rendered ineffective. Further, this inability to approximate \mathbf{Z}_p can be attributed to the unbalanced orthogonal procrustes problem which is unsolved.

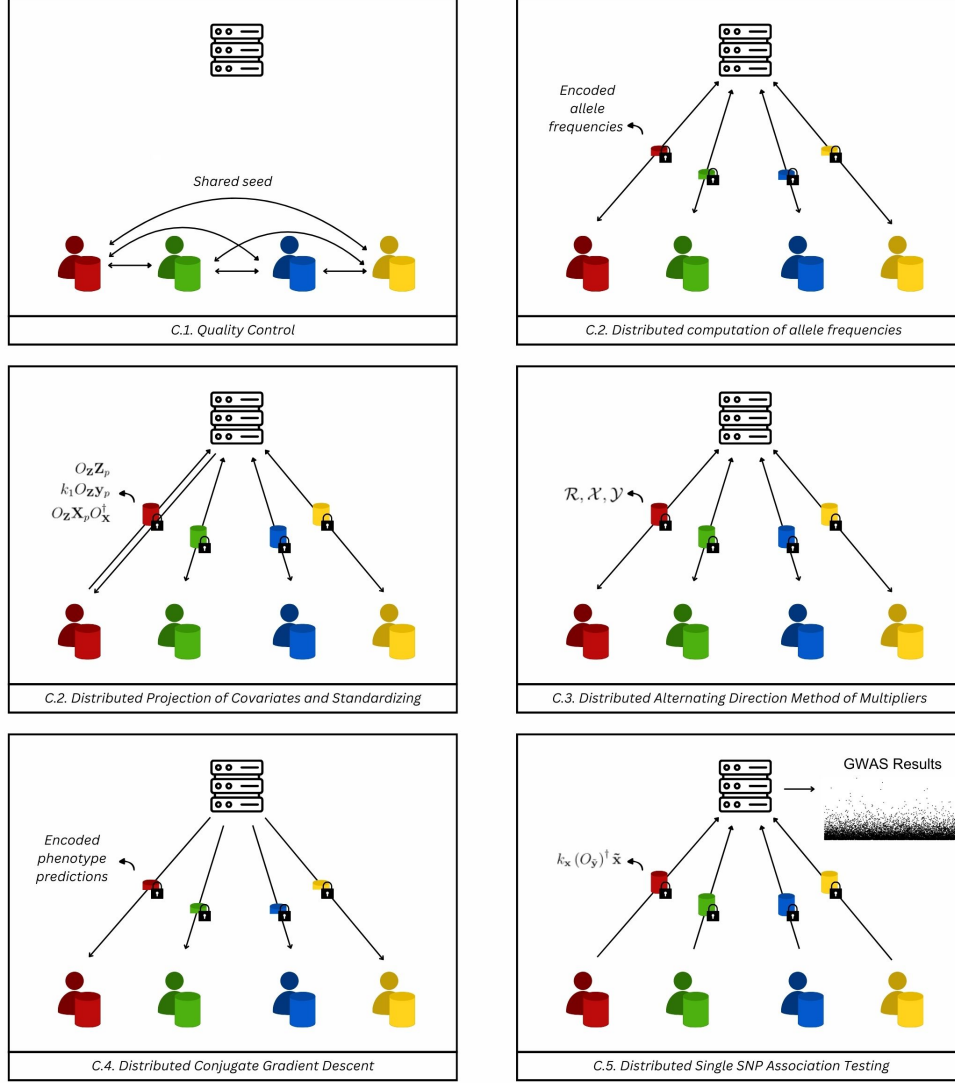


Fig. C1 Step by step illustration of PP-GWAS.

Regarding 2, we see that for a unitary matrix $U \in \mathbb{C}^{(N+kz) \times (N+kz)}$, we have

$$\mathbf{Z}_p^T \mathbf{Z}_p = (U \mathbf{O}_Z \mathbf{Z}_p)^\dagger (U \mathbf{O}_Z \mathbf{Z}_p) = (\mathbf{O}_Z \mathbf{Z}_p)^\dagger (\mathbf{O}_Z \mathbf{Z}_p).$$

As before, $\mathbf{Z}_p^T \mathbf{Z}_p$ is not formed by a unique \mathbf{Z}_p , and the lack of knowledge about the number of samples prohibits the server from learning any more information. As a result, by eigen decomposing $\mathbf{Z}_p^T \mathbf{Z}_p$ the server can only learn the singular values and

singular vectors of \mathbf{Z}_p , which are insufficient to solve for \mathbf{Z}_p . Analogously, the server can't learn anything from the scalar quantities $k_1^2 \mathbf{y}_p^T \mathbf{y}_p$ and $k_x^2 \tilde{\mathbf{x}}_{(test,k,p)}^T \tilde{\mathbf{x}}_{(test,k,p)}$. \square

Theorem 2. *The proposed methodology is secure against a proper subset of semi-honest participants.*

Proof. We define a proper subset of corrupt participants as any subset excluding at least one honest participant. We assume corrupted participants are semi-honest, meaning they follow the protocol but may attempt to learn additional information from the accessible data. Consider the communication protocol within the proposed methodology. Each participant p , only receives the relevant p 'th partitions, such as $E[\tilde{\mathbf{X}}_p]$ and $E[\tilde{\mathbf{y}}_p]$. Therefore if a proper subset of the participants is corrupt, and collude, they cannot access or infer information beyond their encoded partitions. Since our adversarial setting considers a non-colluding semi-honest central server, the server will not deviate from the protocol and share information pertaining to non-corrupt participants with the corrupt participants. \square

Therefore, we have shown that the data of non-corrupt participants remains private, and secure from a proper subset of semi-honest participants, and/or a non-colluding semi-honest central server. Further, the central server does not at any point of the protocol learn the number of samples in the study or the block sizes utilized.

References

- [1] Consortium, T.W.T.C.C.: Genome-wide association study of 14,000 cases of seven common diseases and 3,000 shared controls. *Nature* **447**(7145), 661–678 (2007)
- [2] McCarthy, M.I., Abecasis, G.R., Cardon, L.R., Goldstein, D.B., Little, J., Ioannidis, J.P., Hirschhorn, J.N.: Genome-wide association studies for complex traits: consensus, uncertainty and challenges. *Nature reviews genetics* **9**(5), 356–369 (2008)
- [3] Manolio, T.A., Collins, F.S., Cox, N.J., Goldstein, D.B., Hindorff, L.A., Hunter, D.J., McCarthy, M.I., Ramos, E.M., Cardon, L.R., Chakravarti, A., *et al.*: Finding the missing heritability of complex diseases. *Nature* **461**(7265), 747–753 (2009)
- [4] Graham, S.E., Clarke, S.L., Wu, K.-H.H., Kanoni, S., Zajac, G.J., Ramdas, S., Surakka, I., Ntalla, I., Vedantam, S., Winkler, T.W., *et al.*: The power of genetic diversity in genome-wide association studies of lipids. *Nature* **600**(7890), 675–679 (2021)
- [5] Trubetskoy, V., Pardiñas, A.F., Qi, T., Panagiotaropoulou, G., Awasthi, S., Bigdeli, T.B., Bryois, J., Chen, C.-Y., Dennison, C.A., Hall, L.S., *et al.*: Mapping genomic loci implicates genes and synaptic biology in schizophrenia. *Nature* **604**(7906), 502–508 (2022)
- [6] Peloquin, D., DiMaio, M., Bierer, B., Barnes, M.: Disruptive and avoidable: Gdpr challenges to secondary research uses of data. *European Journal of Human Genetics* **28**(6), 697–705 (2020)
- [7] Staunton, C., Adams, R., Anderson, D., Croxton, T., Kamuya, D., Munene, M., Swanepoel, C.: Protection of personal information act 2013 and data protection for health research in south africa. *International Data Privacy Law* **10**(2), 160–179 (2020)
- [8] Akgün, M., Bayrak, A.O., Ozer, B., Sağiroğlu, M.Ş.: Privacy preserving processing of genomic data: A survey. *Journal of biomedical informatics* **56**, 103–111 (2015)
- [9] Constable, S.D., Tang, Y., Wang, S., Jiang, X., Chapin, S.: Privacy-preserving gwas analysis on federated genomic datasets. In: *BMC Medical Informatics and Decision Making*, vol. 15, pp. 1–9 (2015). Springer
- [10] Bonte, C., Makri, E., Ardeshtirdavani, A., Simm, J., Moreau, Y., Vercauteren, F.: Towards practical privacy-preserving genome-wide association study. *BMC bioinformatics* **19**, 1–12 (2018)
- [11] Cho, H., Wu, D.J., Berger, B.: Secure genome-wide association analysis using multiparty computation. *Nature biotechnology* **36**(6), 547–551 (2018)

- [12] Cho, H., Froelicher, D., Chen, J., Edupalli, M., Pyrgelis, A., Troncoso-Pastoriza, J.R., Hubaux, J.-P., Berger, B.: Secure and federated genome-wide association studies for biobank-scale datasets. *bioRxiv*, 2022–11 (2022)
- [13] Yao, A.C.: Protocols for secure computations. In: 23rd Annual Symposium on Foundations of Computer Science (sfcs 1982), pp. 160–164 (1982). IEEE
- [14] Dwork, C., McSherry, F., Nissim, K., Smith, A.: Calibrating noise to sensitivity in private data analysis. In: Theory of Cryptography: Third Theory of Cryptography Conference, TCC 2006, New York, NY, USA, March 4-7, 2006. Proceedings 3, pp. 265–284 (2006). Springer
- [15] López-Alt, A., Tromer, E., Vaikuntanathan, V.: On-the-fly multiparty computation on the cloud via multikey fully homomorphic encryption. In: Proceedings of the Forty-fourth Annual ACM Symposium on Theory of Computing, pp. 1219–1234 (2012)
- [16] Kuo, M.-H., *et al.*: Opportunities and challenges of cloud computing to improve health care services. *Journal of medical Internet research* **13**(3), 1867 (2011)
- [17] Griebel, L., Prokosch, H.-U., Köpcke, F., Toddenroth, D., Christoph, J., Leb, I., Engel, I., Sedlmayr, M.: A scoping review of cloud computing in healthcare. *BMC medical informatics and decision making* **15**(1), 1–16 (2015)
- [18] Ishai, Y., Kushilevitz, E.: Randomizing polynomials: A new representation with applications to round-efficient secure computation. In: Proceedings 41st Annual Symposium on Foundations of Computer Science, pp. 294–304 (2000). IEEE
- [19] Liu, K., Kargupta, H., Ryan, J.: Random projection-based multiplicative data perturbation for privacy preserving distributed data mining. *IEEE Transactions on knowledge and Data Engineering* **18**(1), 92–106 (2005)
- [20] Mendes, R., Vilela, J.P.: Privacy-preserving data mining: methods, metrics, and applications. *IEEE Access* **5**, 10562–10582 (2017)
- [21] Oliveira, S.R., Zaiane, O.R.: Privacy preserving clustering by data transformation. *Journal of Information and Data Management* **1**(1), 37–37 (2010)
- [22] Nayak, T.K., Sinha, B., Zayatz, L.: Statistical properties of multiplicative noise masking for confidentiality protection. *Journal of Official Statistics* **27**(3), 527 (2011)
- [23] Hannemann, A., Ünal, A.B., Swaminathan, A., Buchmann, E., Akgün, M.: A privacy-preserving framework for collaborative machine learning with kernel methods. In: 2023 5th IEEE International Conference on Trust, Privacy and Security in Intelligent Systems and Applications (TPS-ISA), pp. 82–90 (2023). IEEE

- [24] Mbatches, J., Barnard, L., Backman, J., Marcketta, A., Kosmicki, J.A., Ziyatdinov, A., Benner, C., O’Dushlaine, C., Barber, M., Boutkov, B., *et al.*: Computationally efficient whole-genome regression for quantitative and binary traits. *Nature genetics* **53**(7), 1097–1103 (2021)
- [25] Kadie, C., Heckerman, D.: Ludicrous speed linear mixed models for genome-wide association studies. *BioRxiv*, 154682 (2017)
- [26] Xu, K., Yue, H., Guo, L., Guo, Y., Fang, Y.: Privacy-preserving machine learning algorithms for big data systems. In: 2015 IEEE 35th International Conference on Distributed Computing Systems, pp. 318–327 (2015). IEEE
- [27] Jackson, C.: sparse-dot-mkl: Intel MKL wrapper for sparse matrix multiplication. https://github.com/flatironinstitute/sparse_dot. Accessed: September 2023 (2023)
- [28] Ayres, D.L., Darling, A., Zwickl, D.J., Beerli, P., Holder, M.T., Lewis, P.O., Huelsenbeck, J.P., Ronquist, F., Swofford, D.L., Cummings, M.P., *et al.*: Beagle: an application programming interface and high-performance computing library for statistical phylogenetics. *Systematic biology* **61**(1), 170–173 (2012)
- [29] Loh, P.-R., Kichaev, G., Gazal, S., Schoech, A.P., Price, A.L.: Mixed-model association for biobank-scale datasets. *Nature genetics* **50**(7), 906–908 (2018)
- [30] Jiang, L., Zheng, Z., Qi, T., Kemper, K.E., Wray, N.R., Visscher, P.M., Yang, J.: A resource-efficient tool for mixed model association analysis of large-scale data. *Nature genetics* **51**(12), 1749–1755 (2019)
- [31] Zhou, W., Nielsen, J.B., Fritsche, L.G., Dey, R., Gabrielsen, M.E., Wolford, B.N., LeFaive, J., VandeHaar, P., Gagliano, S.A., Gifford, A., *et al.*: Efficiently controlling for case-control imbalance and sample relatedness in large-scale genetic association studies. *Nature genetics* **50**(9), 1335–1341 (2018)
- [32] Lippert, C., Listgarten, J., Liu, Y., Kadie, C.M., Davidson, R.I., Heckerman, D.: Fast linear mixed models for genome-wide association studies. *Nature methods* **8**(10), 833–835 (2011)
- [33] Wittkowski, K.M., Sonakya, V., Bigio, B., Tonn, M.K., Shic, F., Ascano, M., Nasca, C., Simson, G.-V., *et al.*: A novel computational biostatistics approach implies impaired dephosphorylation of growth factor receptors as associated with severity of autism. *Translational psychiatry* **4**(1), 354–354 (2014)
- [34] Hyvärinen, A., Oja, E.: Independent component analysis: algorithms and applications. *Neural networks* **13**(4-5), 411–430 (2000)
- [35] Lee, T.-W.: Independent Component Analysis: Theory and Applications. Springer, ??? (2013)

- [36] Zhang, Z., Qiu, Y., Du, K.: Conditions for optimal solutions of unbalanced procrustes problem on stiefel manifold. *Journal of Computational Mathematics*, 661–671 (2007)
- [37] Ding, A.A., Miao, G., Wu, S.S.: On the privacy and utility properties of triple matrix-masking. *The Journal of privacy and confidentiality* **10**(2) (2020)
- [38] Boyd, S., Parikh, N., Chu, E., Peleato, B., Eckstein, J., *et al.*: Distributed optimization and statistical learning via the alternating direction method of multipliers. *Foundations and Trends® in Machine learning* **3**(1), 1–122 (2011)
- [39] Ünal, A.B., Akgün, M., Pfeifer, N.: Escaped: Efficient secure and private dot product framework for kernel-based machine learning algorithms with applications in healthcare. In: *Proceedings of the AAAI Conference on Artificial Intelligence*, vol. 35, pp. 9988–9996 (2021)
- [40] Hannemann, A., Swaminathan, A., Ünal, A.B., Akgün, M.: Privacy-preserving Distributed Kernel Learning for Medical Image Analysis. *Manuscript under review* (2024)